

Free Convection from a Rotating Vertical Porous Plate in a Dissipative Micropolar Fluid with Cross Diffusion Effects

*Shamshuddin M.D., **Siva Reddy Sheri

*Department of Mathematics, Vaagdevi College of Engineering (autonomous), Warangal-506005, Telangana State, India. (shammaths@gmail.com)

**Department of Mathematics, GITAM University, Hyderabad Campus, Telangana, India.

Abstract

A numerical analysis is conducted for the primary and secondary flow characterizing dissipative micropolar convective heat and mass transfer from a rotating vertical plate with oscillatory plate velocity adjacent to a permeable medium. A dominant cross diffusion so called Soret and Dufour effects has been included. The entire system rotates with uniform angular velocity about an axis normal to the plate. Rosseland's diffusion approximation is used to describe the radiative heat flux in the energy equation. The partial differential equations governing the flow problem are rendered dimensionless with appropriate transformation variables. They exhibit both primary and secondary motions when the boundaries are subject to slow rotations. A Galerkin finite element method is employed to solve the emerging multi-physical fluid dynamics problem. The evolution of primary and secondary velocity, primary and secondary angular velocity, temperature and concentration are examined for a variety of parameters which governs the flow. Comparison of the present numerical solutions with the earlier published analytical results shows an excellent agreement, this validating the accuracy of the present numerical method. The current simulations may be applicable to various oscillating rheometry, magnetic rheo-dynamic materials processing systems and rotating MHD energy generator near-wall flows.

Key words

Viscous dissipation, Soret and Dufour effect, Micropolar fluid, Galerkin finite element method, rotating plate.

1. Introduction

In many physico-heat and mass transfer studies, related to both Newtonian and non-Newtonian fluids, thermo-diffusion (Soret) and diffusio-thermo (Dufour) effects play a prominent role. These effects are often of smaller order of magnitude in comparison with the diffusive effects associated with thermal conduction (Fourier's law) and mass diffusion (Fick's laws) and are frequently neglected. However, these so-called cross diffusion effects become important if not dominant, in materials processing operations e.g. dendritic growth [1-2], magnetic separation of colloids [3], MHD power generators [4] and aerospace combustion and flame dynamics [5-6] where they arise in binary gas and supercritical fuel injection systems. Generally, when heat and mass transfer effects occur simultaneously in a moving fluid, the relationship between the fluxes and the driven potentials become significant. An energy flux can be generated not only by temperature gradient but also by composition gradient as well. The energy caused by a composition gradient is called the Dufour effect or diffusion-thermo effect. The energy caused by a temperature gradient is called the Soret effect or thermo-diffusion effect. The thermal Soret effect can for example also generate a very strong coupling force between the species (solute) and heat transport. Due to the significance importance of Soret and Dufour diffusion phenomena for fluids with medium molecular weight as well as very light molecular weights, in recent years, substantial interest has emerged in simulation of these effects in many multi-physical transport problems. Postelnicu [7] considered magnetic free convection in porous media with Soret and Dufour effects. Alam and Rahman [8] investigated combined Dufour and Soret effects on hydromagnetic natural convection flow in a porous medium. Further studies of Newtonian flows with Soret/Dufour effects include Vasu et al. [9] (for wall mass flux effects), Bég et al. [10] and Thirpathy et al. [11] (for hydromagnetic flow from an extending sheet in porous media) and Partha et al. [12] (for non-Darcian thermal convection). Non-Newtonian heat and mass transfer with Soret and/or Dufour effects has also attracted some attention. Bég et al. [13] used a finite element method to simulate two-dimensional micropolar boundary layer flows in Darcy-Forchheimer permeable materials with Soret and Dufour cross diffusion effects. Other representative studies include Mishra et al. [14], Olajuwon and Oahimire [15], Kundu et al. [16], Bakr and Chamkha [17] (again both for micropolar fluids). Cross diffusion effects with higher order chemical reaction effects on micropolar fluid was examined by Arifuzzaman et al. [18].

Rotating thermal convection flows arise in an extensive range of industrial systems including rotating heat exchangers, multi-stage cyclone separators, mixing devices in chemical engineering and spin-stabilization of spacecraft vehicles. Rotating fluid systems generate both real and fictitious forces, the former is the centrifugal force and the latter is the Coriolis force. Should the rate of

rotation of a body change then a third fictitious force, the Euler force may also be invoked. The interplay between Coriolis force and viscous force have profound effects on for example external boundary layer growth, thermal boundary layer thickness etc. The Coriolis force induces motion in the secondary flow direction. Further complexities arise when the fluid is electrically conducting and when mass transfer (species diffusion) is present. Investigations of boundary layer flows with variety of configurations e.g. rotating plate [19], co-rotating cylinder [20], rotating disk [21], rotating system [22, 23]. These studies have shown significant modification in momentum, heat and also mass transfer rates induced by rotational body force. They have however generally been confined to Newtonian fluids. Many non-Newtonian fluids arise in technological applications including polymers, slurries, gels, dusty suspensions etc. They are characterized by complex micro-structure and observations have revealed that such fluids generally deviate from the classical Navier-Stokes viscous flow model. This model cannot simulate the effects of molecular spin since it neglects couple stresses in the constitutive formulation. To address this issue Eringen proposed the micro-morphic theory of fluids over five decades ago, of which several special cases have sustained significant interest in engineering sciences. These are the micro-stretch fluid and the micropolar fluid [24]. The latter has received wide attention in heat and mass transfer modelling. The Eringen micropolar theory features additional degrees of freedom (gyratory motions) which allow the physical representation of the rotation of the microstructure. Hence, the balance law of angular momentum is introduced for solving gyration, extending the conventional linear momentum balance in Newtonian models. Molecular spin can therefore be analysed robustly within the framework of micropolar fluid mechanics. An additional advantage is that micropolar models do not require computationally intensive simulations which are necessary for alternative approaches in micro scale fluid dynamics (e.g. Molecular Dynamics, Monte Carlo simulation etc.). Micropolar fluids do not sustain a simple shearing motion, where only one component of velocity is present. In the context of rotating flows, they provide both an assessment of the micro-scale rotary motions and also the influence of micro-structural characteristics on global rotational motions. The interest in the present novel investigation arises from a desire to elaborate the collective influence of primary and secondary flow from a spinning rigid body (plate) when the boundaries are subjected to slow rotation. Largely motivated by geophysical and petrochemical engineering systems, early studies of micropolar transport phenomena from rotating bodies were presented by Rao *et al.* [25], Ramkissoon [26], Kirwan and Chang [27] and Sastry and Rao [28]. Few recent related studies of micropolar and nano fluid transport from stretching surface are presented by Mohanty *et al.* [29], Mishra *et al.* [30], Rout *et al.* [31], Baag *et al.* [32]. Arifuzzaman *et al.* [33], Bég *et al.* [34], also Williamson fluid flow behaviour for linearly stretched surface was

examined by Khan et al. [35]. These investigations were however confined to fluid flow showing that generally the presence of micropolar elements enhances momentum boundary layer thickness. One of the earliest comprehensive analyses of micropolar thermal convection from a spinning body was conducted by Gorla and Takhar [36] who also considered heat generation effects. They showed numerically that the momentum, angular momentum (gyration) and thermal boundary layers grow with centrifugal forces. Gorla [37] subsequently analyzed the non-similar mixed convection of a micropolar fluid from a rotating cone, exploring the influence of microrotation boundary conditions on velocity, micro-rotation and heat transfer distributions. The rotationally symmetric flow of micropolar fluids from a rotating disk was studied by Nazir et al. [38] using the successive over relaxation (SOR) method. Deng et al. [39] presented effects of pipe rotation on dynamic hydro cyclone. Very recently Gajjela et al. [40] derived analytical solutions for Bejan number in magnetized micropolar rotating annular flow. Periodic magnetic field effect on gray nanofluid using EFD (explicit finite difference method) was studied by Biswas et al. [41]. Maxwell fluid flow in presence of nano-particle was examined by Arifuzzaman et al. [42]. Jeffrey fluid flow with the impact of thermal radiation and Joule heating was analyzed by Kumar et al. [43] Entropy generation analysis for radiative micropolar fluid was presented by Srinivas et al. [44].

These simulations have generally considered steady-state flows. However, many materials processing systems feature oscillatory flow characteristics induced by periodic motions of the boundary. Periodic flows and judicious selection of oscillation frequency can aid in the diffusion of species and transport of heat. This can be critical in certain flow reactor designs using non-Newtonian liquids [45]. Many theoretical studies on oscillatory multi-physical flows have been communicated in recent years. Bég et al. [46] derived asymptotic solutions for oscillatory Couette channel hydromagnetic flow with inclined magnetic field and porous medium drag effects. Reis et al. [47] reported both analytical and experimental results for unsteady oscillatory hydrodynamics in a screening reactor. Bhargava et al. [48] presented finite element solutions for periodic reactive flow, heat and mass diffusion in porous media with cross diffusion effects. Bég et al. [49] obtained asymptotic solutions for oscillating hydromagnetic flow and heat transfer in couple stress liquids in a spinning bioreactor channel configuration. Maqbool et al. [50] presented Fourier series solutions for a variety of oscillatory magnetohydrodynamic channel flows, also considering rotational body force and both Newtonian and non-Newtonian material models. Oscillatory micropolar flows in the annular region of two concentric spheres were examined by Iynger and Geeta vani [51]. Nayak et al. [52] examined buoyancy effects in free convective MHD flow. Buoyancy effects on magnetic oscillatory flow of micropolar fluids were reported by Kim and Lee

[53] and Modather et al. [54]. Shamsuddin et al. [55] computed cross-diffusion effects on transient dissipative micropolar free convection flows using a finite element technique.

In the present investigation we generalize and extend existing studies [15,16,17,18] to consider the combined effects of Soret and Dufour cross diffusion and viscous dissipation on radiative magnetohydrodynamic micropolar flow, heat and mass transfer from a rotating vertical plate adjacent to a porous medium. The non-dimensional conservation equations are solved with a Galerkin finite element method. The effect of various physical parameters on the translational primary and secondary velocity, primary and secondary micro-rotation velocity, temperature and concentration profiles as well as on local skin friction coefficient, wall couple stress, Sherwood number and Nusselt number are tabulated. Validation of the analysis has been performed by comparing the present results with those of [15,16, 17]. The current study is relevant to high temperature electromagnetic rheological flows in energy generators and magneto-rheological materials fabrication systems (where thermal radiation heat transfer is also significant) and has not appeared in technical literature thus far.

2. Mathematical Modelling

Unsteady natural convective flow, heat and mass transfer of an electrically conducting incompressible micro-polar fluid from a vertical plane considered. The vertical plate is assumed to be subjected to a constant heat flux, q_w and a constant concentration gradient, m_w also plate and fluid like in the $x'-z'$ plane and both are rotating in unison with constant uniform angular velocity Ω about the z' -axis with a velocity $u' = U_r(1 + \varepsilon \cos n't')$. Initially at time $t' \leq 0$ both the plate and fluid are at rest and are maintained at a uniform temperature T_∞ and concentration C_∞ . At time $t' > 0$, the plate starts moving in the x' -direction with uniform velocity U_r in its own plane, thereafter the plate is maintained at constant temperature T_w and concentration C_w . These values are assumed to be greater than the ambient temperature T_∞ and concentration C_∞ . The physical configuration is illustrated in Fig. 1. Darcy's law is assumed which is valid for low Reynolds number transport. A magnetic field of uniform strength B_0 is applied in a direction parallel to the z' axis which is perpendicular to the flow direction. It is assumed that in comparison to the applied magnetic field, induced magnetic field is negligible. The magnetohydrodynamic (MHD) body force term is derived from an order of magnitude analysis of the full Navier-Stokes equation. It is also assumed that applied or polarized voltage is neglected so that no energy is added or extracted from the fluid by electrical means. The fluid is considered to be a gray, absorbing-emitting but non-scattering medium and the Rosseland approximation is used to describe the radiative heat flux. The radiative

The energy equation

$$\frac{\partial T}{\partial t'} + w' \frac{\partial T}{\partial z'} = \left(\alpha + \frac{16 \bar{\sigma} T_\infty^3}{3 \bar{k} \rho C_p} \right) \frac{\partial^2 T}{\partial z'^2} + \frac{1}{C_p} (v + v_r) \left[\left(\frac{\partial u'}{\partial z'} \right)^2 + \left(\frac{\partial \omega'}{\partial z'} \right)^2 \right] + \frac{D_m K_T}{C_s C_p} \left(\frac{\partial^2 C}{\partial z'^2} \right) \quad (6)$$

The concentration equation

$$\frac{\partial C}{\partial t'} + w' \frac{\partial C}{\partial z'} = D_m \left(\frac{\partial^2 C}{\partial z'^2} \right) + \frac{D_m K_t}{T_m} \left(\frac{\partial^2 T}{\partial z'^2} \right) \quad (7)$$

The following spatial and temporal boundary conditions are prescribed as

$$\left. \begin{aligned} \left\{ \begin{array}{l} t' \leq 0 : u' = v' = 0 \quad \bar{\omega}'_1 = \bar{\omega}'_2 = 0 \quad T = T_\infty, C = C_\infty \\ t' > 0 : u' = U_r \left[1 + \frac{\varepsilon}{2} \left(e^{in't'} + e^{-in't'} \right) \right], v' = 0, \quad \bar{\omega}'_1 = \frac{-1}{2} \frac{\partial v}{\partial z'}, \bar{\omega}'_2 = \frac{1}{2} \frac{\partial u}{\partial z'} \\ (T')_{z'=0} = -\frac{q_w}{\kappa}, \quad (C')_{z'=0} = -\frac{m_w}{D_m} \quad \text{at } z' = 0 \\ \text{and} \\ u' = v' = 0 \quad \bar{\omega}'_1 = \bar{\omega}'_2 = 0, T = T_\infty, C = C_\infty \quad \text{as } z' \rightarrow \infty \end{array} \right\} \end{aligned} \right\} \quad (8)$$

The oscillatory plate velocity assumed in Eq. (8) is based on [56], Integrating the continuity equation (1) for variable transpiration (lateral mass flux) velocity normal to the plate, a convenient solution emerges as:

$$w' = -w_0 \quad (9)$$

Where w_0 is the normal velocity at the plate $w_0 > 0$ for suction, $w_0 < 0$ for blowing and $w_0 = 0$ for impermeable plate, Introducing the following non-dimension variables

$$\left. \begin{aligned} z' = \frac{z U_r}{v}, u' = \frac{u}{U_r}, v' = \frac{v}{U_r}, t' = \frac{t U_r^2}{v}, n' = \frac{nv}{U_r^2}, \bar{\omega}'_1 = \frac{\omega_1 v}{U_r^2}, \bar{\omega}'_2 = \frac{\omega_2 v}{U_r^2}, \theta = \frac{\kappa(T - T_\infty)}{q_w}, \\ \varphi = \frac{Dm(C - C_\infty)}{m_w}, R = \frac{2\Omega v}{U_r^2}, M = \frac{\sigma B_o^2 v}{\rho U_r^2}, K = \frac{\kappa U_r^2}{v^2}, Gr = \frac{vg\beta_T q_w}{\kappa U_r^3}, Gm = \frac{v g\beta_C M_w}{Dm U_r^3}, \\ S = \frac{w_0}{U_r}, Pr = \frac{\mu \rho C_p}{\kappa}, Sc = \frac{v}{Dm}, F = \frac{16 \bar{\sigma} T_\infty^3}{3 \bar{k}}, Ec = \frac{U_r^2}{C_p(T_w - T_\infty)}, Du = \frac{\kappa^2 K_t m_w}{q_w \rho c \mu}, \\ Sr = \frac{Dm K_t q_w}{m_w \kappa}, \Delta = \frac{K}{\rho v}, \lambda = \frac{\gamma}{\mu j} = \left(1 + \frac{\Delta}{2} \right), \end{aligned} \right\} \quad (10)$$

Using dimensionless variables (10) into equations (1) - (7) yield the following dimensionless partial differential equations

$$\frac{\partial u}{\partial t} - S \frac{\partial u}{\partial z} - Rv = (1 + \Delta) \frac{\partial^2 u}{\partial z^2} + Gr\theta + Gm\varphi - \left(M + \frac{1}{K} \right) u - \Delta \frac{\partial \omega_2}{\partial z} \quad (11)$$

$$\frac{\partial v}{\partial t} - S \frac{\partial v}{\partial z} + Ru = (1 + \Delta) \frac{\partial^2 v}{\partial z^2} - \left(M + \frac{1}{K} \right) v + \Delta \frac{\partial \omega_1}{\partial z} \quad (12)$$

$$\frac{\partial \omega_1}{\partial t} - S \frac{\partial \omega_1}{\partial z} = \lambda \frac{\partial^2 \omega_1}{\partial z^2} \quad (13)$$

$$\frac{\partial \omega_2}{\partial t} - S \frac{\partial \omega_2}{\partial z} = \lambda \frac{\partial^2 \omega_2}{\partial z^2} \quad (14)$$

The decoupling form for both Dufour and Soret effects (cross diffusion equations) are as follows

$$\frac{\partial^2 \theta}{\partial z^2} = \frac{Pr}{(1+F) - Sc Sr Pr Du} \left(\frac{\partial \theta}{\partial t} - Du Sc \frac{\partial \phi}{\partial t} - S \frac{\partial \theta}{\partial z} + S Du Sc \frac{\partial \phi}{\partial z} - (1 + \Delta) Ec \left[\left(\frac{\partial u}{\partial z} \right)^2 + \left(\frac{\partial \omega}{\partial z} \right)^2 \right] \right) \quad (15)$$

$$\frac{\partial^2 \phi}{\partial z^2} = \frac{-Sc}{(1+F) - Sc Sr Pr Du} \left(Pr Sr \frac{\partial \theta}{\partial t} - (1+F) \frac{\partial \phi}{\partial t} - S Pr Sr \frac{\partial \theta}{\partial z} + (1+F) S \frac{\partial \phi}{\partial z} - Pr Sr (1 + \Delta) Ec \left[\left(\frac{\partial u}{\partial z} \right)^2 + \left(\frac{\partial \omega}{\partial z} \right)^2 \right] \right) \quad (16)$$

The boundary conditions can be written in non-dimensional form as follows:

$$\left. \begin{array}{l} \text{for } t \leq 0: \quad u = v = 0 \quad \bar{\omega}_1 = \bar{\omega}_2 = 0 \quad \theta = 0, \phi = 0 \\ \text{for } t > 0: \quad u = \left[1 + \frac{\varepsilon}{2} \left(e^{int} + e^{-int} \right) \right], v = 0, \bar{\omega}_1 = \frac{-1}{2} \frac{\partial v}{\partial z}, \bar{\omega}_2 = \frac{1}{2} \frac{\partial u}{\partial z} \\ \theta' = -1, \phi' = -1 \quad \text{at } z = 0 \quad \text{and} \\ u = v = 0 \quad \bar{\omega}_1 = \bar{\omega}_2 = 0 \quad \theta = \phi = 0 \quad \text{as } z \rightarrow \infty \end{array} \right\} \quad (17)$$

For materials processing operations, the physical quantities of principal interest are the wall skin-friction components (plate shear stress), wall couple stress components (micro-rotation gradient), Nusselt number (wall heat transfer rate) and Sherwood number (wall mass transfer rate): Skin-friction components (primary and secondary) are obtained as:

$$Cf = \frac{\tau'_w}{\rho U_r^2} = \frac{(Cfx + Cfy)}{\rho U_r^2} \quad (18)$$

$$\text{where } Cfx = \left((\mu + K) \frac{\partial u'}{\partial z'} + K \omega'_1 \right)_{z'=0} = \rho U_r^2 \left[(1 + \Delta) \frac{\partial u}{\partial z} - \frac{\Delta}{2} \frac{\partial v}{\partial z} \right]_{z=0};$$

$$Cfy = \left((\mu + K) \frac{\partial v}{\partial z} + K \omega'_2 \right)_{z'=0} = \rho U_r^2 \left[(1 + \Delta) \frac{\partial v}{\partial z} + \frac{\Delta}{2} \frac{\partial u}{\partial z} \right]_{z=0}$$

$$Cw = (Cwx + iCwy) = \frac{(Mwx + iMwy) v^2}{\gamma U_r^3} \quad (19)$$

$$\text{where } M_{wx} = \gamma \left(\frac{\partial \omega_1'}{\partial z'} \right)_{z'=0} = \frac{\gamma U_r^3}{\nu^2} \left(\frac{\partial \omega_1}{\partial z} \right); \quad C_{wx} = \frac{M_{wx} \nu^2}{\gamma U_r^3} = \left(\frac{\partial \omega_1}{\partial z} \right)_{z=0};$$

$$M_{wy} = \gamma \left(\frac{\partial \omega_2'}{\partial z'} \right)_{z'=0} = \frac{\gamma U_r^3}{\nu^2} \left(\frac{\partial \omega_2}{\partial z} \right); \quad C_{wy} = \frac{M_{wy} \nu^2}{\gamma U_r^3} = \left(\frac{\partial \omega_2}{\partial z} \right)_{z=0}$$

In addition to that rate of heat transfer and rate of mass transfer at the surface of wall are

$$Nu = -x \left(\frac{\partial T / \partial z}{\kappa (T_\infty - T_w)} \right)_{z'=0} \quad (20)$$

$$Sh = -x \left(\frac{\partial C / \partial z}{Dm (C_\infty - C_w)} \right)_{z'=0} \quad (21)$$

Converting (18)- (21) in non-dimensional for are obtained as follows

Skin-friction components (primary and secondary) are obtained as

$$C_{f_x} = \rho U_r^2 \left[(1 + \Delta) \frac{\partial u}{\partial z} - \frac{\Delta}{2} \frac{\partial v}{\partial z} \right], \quad C_{f_y} = \rho U_r^2 \left[(1 + \Delta) \frac{\partial v}{\partial z} + \frac{\Delta}{2} \frac{\partial u}{\partial z} \right] \quad (22)$$

Wall couple stress components (primary and secondary) are computed as:

$$C_{wx} = \left[\frac{\partial \omega_1}{\partial z} \right]_{z=0}, \quad C_{wy} = \left[\frac{\partial \omega_2}{\partial z} \right]_{z=0} \quad (23)$$

The plate surface rate of the heat transfer i.e. Nusselt number emerges as:

$$Nu = \frac{Re_x}{\theta(0)} \quad (24)$$

The plate surface rate of mass transfer i.e. Sherwood number is calculated with:

$$Sh = \frac{Re_x}{\phi(0)} \quad (25)$$

Where $Re_x = U_r x / \nu$ is the local Reynolds number, it is important to note that the present simulation extends the conventional studies by including a secondary component for the wall couple stress function. This allows further sophistication in analyzing the micro-element gyration field near the plate surface, a characteristic which is usually only addressed by a single couple stress function as noted by Eringen and many others. we also note that the micro-rotation boundary conditions in (17) reflect the physically realistic conditions wherein the wall gradient of the gyration vector must approach zero at the wall. This accommodates the framework of boundary layer growth at the wall, which is violated by the often-simple reduction to a vanishing micro-rotation boundary condition. Micro-element rotary motions will be inhibited at the wall but not completely eliminated. The micropolar theory model's fluids comprising non-deformable micro-

elements. The local effect arising from the intrinsic motion and the microstructure of fluid elements in micropolar fluids are therefore taken into account not only in the angular momenta field equations but also in the boundary conditions (17).

3. Finite Element Solution

3.1 Finite Element Method

The set of time-dependent, reduced, non-dimensional, coupled partial differential equations (24) -(27) subject to boundary conditions (28) are nonlinear, coupled and therefore cannot be solved analytically. It is equally versatile at solving Newtonian and non-Newtonian problems. The variational form is particularly popular for fluid mechanics simulations and general details of this methodology are available in many textbooks Reddy [57], Bathe [58]. Some recent examples of applications with associated computational details of finite element modelling of non-Newtonian magnetohydrodynamic flows include unsteady micropolar flow studies employing FEM include magnetic micropolar nanofluid cavity flow [59] and micropolar flow from an oblique surface [60].

- Discretization of the infinite fluid domain into finite elements
- Derivation of element equations
- Assembly of Element Equations
- Imposition of boundary conditions
- Solution of assembled equations

3.2 Variational Formulation

The variational formulation associated with Eqs. (11) - (16) over a typical two-node linear element (z_e, z_{e+1}) is given by:

$$\int_{z_e}^{z_{e+1}} w_1 \left[\frac{\partial u}{\partial t} - S \frac{\partial u}{\partial z} - Rv - (1 + \Delta) \frac{\partial^2 u}{\partial z^2} - (Gr\theta + Gm\varphi) + A_1 u + \Delta \frac{\partial \omega_2}{\partial z} \right] dz = 0 \quad (26)$$

$$\int_{z_e}^{z_{e+1}} w_2 \left[\frac{\partial v}{\partial t} - S \frac{\partial v}{\partial z} + Ru - (1 + \Delta) \frac{\partial^2 v}{\partial z^2} + A_1 v - \Delta \frac{\partial \omega_1}{\partial z} \right] dz = 0 \quad (27)$$

$$\int_{z_e}^{z_{e+1}} w_3 \left[\frac{\partial \omega_1}{\partial t} - S \frac{\partial \omega_1}{\partial z} - \lambda \frac{\partial^2 \omega_1}{\partial z^2} \right] dz = 0 \quad (28)$$

$$\int_{z_e}^{z_{e+1}} w_4 \left[\frac{\partial \omega_2}{\partial t} - S \frac{\partial \omega_2}{\partial z} - \lambda \frac{\partial^2 \omega_2}{\partial z^2} \right] dz = 0 \quad (29)$$

$$\int_{z_e}^{z_{e+1}} w_5 \left[\begin{aligned} & \frac{\partial^2 \theta}{\partial z^2} - A_2 \frac{\partial \theta}{\partial t} + A_2 Du Sc \frac{\partial \varphi}{\partial t} + A_2 S \frac{\partial \theta}{\partial z} - A_2 S Du Sc \frac{\partial \varphi}{\partial z} \\ & - A_2 Ec (1 + \Delta) \left[\left(\frac{\partial u}{\partial z} \right)^2 + \left(\frac{\partial \omega}{\partial z} \right)^2 \right] \end{aligned} \right] dz = 0 \quad (30)$$

$$\int_{z_e}^{z_{e+1}} w_6 \left[\begin{aligned} & \frac{\partial^2 \varphi}{\partial z^2} - A_3 Pr Sr \frac{\partial \theta}{\partial t} + A_3 (1 + F) \frac{\partial \varphi}{\partial t} + A_3 S Pr Sr \frac{\partial \theta}{\partial z} - A_3 (1 + F) S \frac{\partial \varphi}{\partial z} \\ & + A_3 Pr Sr Ec (1 + \Delta) \left[\left(\frac{\partial u}{\partial z} \right)^2 + \left(\frac{\partial \omega}{\partial z} \right)^2 \right] \end{aligned} \right] dz = 0 \quad (31)$$

Here w_1, w_2, w_3, w_4, w_5 and w_6 are arbitrary test functions and may be viewed as the variations in $u, v, \omega_1, \omega_2, \theta$, and φ respectively, and $A_1 = \left(M + \frac{1}{K} \right)$, $A_2 = \frac{Pr}{(1 + F) - Sc Sr Pr Du}$,

$A_3 = \frac{-Sc}{(1 + F) - Sc Sr Pr Du}$. After dropping the order of integration and non-linearity, we arrive at

the following system of equations:

$$\int_{z_e}^{z_{e+1}} \left[w_1 \frac{\partial u}{\partial t} - Sw_1 \frac{\partial u}{\partial z} - Rw_1 v - (1 + \Delta)w_1 \frac{\partial w_1}{\partial z} \frac{\partial u}{\partial z} - (Grw_1 \theta + Gmw_1 \varphi) + A_1 w_1 u + \Delta w_1 \frac{\partial \omega_2}{\partial z} \right] dz - \left[w_1 \left(\frac{\partial u}{\partial z} \right) \right]_{z_e}^{z_{e+1}} = 0 \quad (32)$$

$$\int_{z_e}^{z_{e+1}} \left[w_2 \frac{\partial v}{\partial t} - Sw_2 \frac{\partial v}{\partial z} + Rw_2 u - (1 + \Delta)w_2 \frac{\partial w_2}{\partial z} \frac{\partial v}{\partial z} + A_1 w_2 v - \Delta \frac{\partial \omega_1}{\partial z} \right] dz - \left[w_2 \left(\frac{\partial v}{\partial z} \right) \right]_{z_e}^{z_{e+1}} = 0 \quad (33)$$

$$\int_{z_e}^{z_{e+1}} \left[w_3 \frac{\partial \omega_1}{\partial t} - Sw_3 \frac{\partial \omega_1}{\partial z} - \lambda \frac{\partial w_3}{\partial z} \frac{\partial \omega_1}{\partial z} \right] dz - \left[w_3 \left(\frac{\partial \omega_1}{\partial z} \right) \right]_{z_e}^{z_{e+1}} = 0 \quad (34)$$

$$\int_{z_e}^{z_{e+1}} \left[w_4 \frac{\partial \omega_2}{\partial t} - Sw_4 \frac{\partial \omega_2}{\partial z} - \lambda \frac{\partial w_4}{\partial z} \frac{\partial \omega_2}{\partial z} \right] dz - \left[w_4 \left(\frac{\partial \omega_2}{\partial z} \right) \right]_{z_e}^{z_{e+1}} = 0 \quad (35)$$

$$\int_{z_e}^{z_{e+1}} \left[\begin{aligned} & \frac{\partial w_5}{\partial z} \frac{\partial \theta}{\partial z} - A_2 w_5 \frac{\partial \theta}{\partial t} + A_2 Du Sc w_5 \frac{\partial \varphi}{\partial t} + A_2 S w_5 \frac{\partial \theta}{\partial z} \\ & - A_2 S Du Sc w_5 \frac{\partial \varphi}{\partial z} - A_2 Ec (1 + \Delta) w_5 \left[\left(\frac{\partial \bar{u}}{\partial z} \right) \left(\frac{\partial u}{\partial z} \right) + \left(\frac{\partial \omega}{\partial z} \right)^2 \right] \end{aligned} \right] dz - \left[w_5 \left(\frac{\partial \theta}{\partial z} \right) + Duw_5 \left(\frac{\partial \varphi}{\partial z} \right) \right]_{z_e}^{z_{e+1}} = 0 \quad (36)$$

$$\int_{z_e}^{z_{e+1}} \left[\begin{aligned} & \frac{\partial w_6}{\partial z} \frac{\partial \varphi}{\partial z} - A_3 w_6 Pr Sr \frac{\partial \theta}{\partial t} + A_3 (1 + F) w_6 \frac{\partial \varphi}{\partial t} + A_3 S Pr Sr w_6 \frac{\partial \theta}{\partial z} \\ & - A_3 (1 + F) S w_6 \frac{\partial \varphi}{\partial z} + A_3 Pr Sr Ec (1 + \Delta) w_6 \left[\left(\frac{\partial \bar{u}}{\partial z} \right) \left(\frac{\partial u}{\partial z} \right) + \left(\frac{\partial \omega}{\partial z} \right)^2 \right] \end{aligned} \right] dz - \left[w_6 \left(\frac{\partial \varphi}{\partial z} \right) + Srw_6 \left(\frac{\partial \theta}{\partial z} \right) \right]_{z_e}^{z_{e+1}} = 0 \quad (37)$$

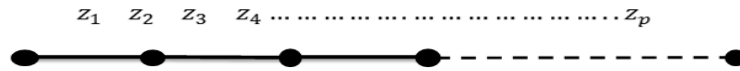
3.3 Finite Element Formulation

The finite element model may be obtained from Eqs. (32) - (37) by substituting finite element approximations of the form:

$$u = \sum_{j=1}^p u_j^e \psi_j^e, v = \sum_{j=1}^p v_j^e \psi_j^e, \omega_1 = \sum_{j=1}^p \omega_{1j}^e \psi_j^e, \omega_2 = \sum_{j=1}^p \omega_{2j}^e \psi_j^e, \theta = \sum_{j=1}^p \theta_j^e \psi_j^e, \phi = \sum_{j=1}^p \phi_j^e \psi_j^e \quad (38)$$

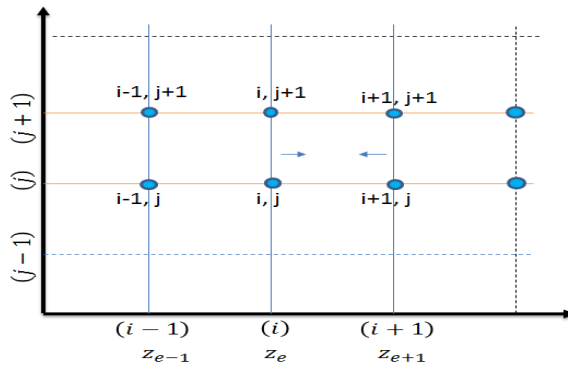
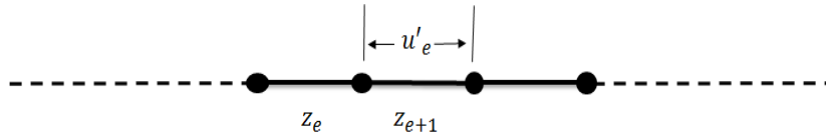
With $w_1 = w_2 = w_3 = w_4 = w_5 = w_6 = \psi_j^e$ ($i=1, 2, \dots, p$), where $u_j^e, v_j^e, \omega_{1j}^e, \omega_{2j}^e, \theta_j^e$ and ϕ_j^e are flow velocities, microrotational velocities, temperature and concentration magnitudes respectively at the j^{th} node of typical e^{th} element (z_e, z_{e+1})

In our computations, the shape functions for a typical element (z_e, z_{e+1}) , the global coordinates are represented as below



Where $\psi_i = \frac{(z - z_1)(z - z_2)(z - z_3)(z - z_4) \dots (z - z_p)}{(z_i - z_1)(z_i - z_2)(z_i - z_3)(z_i - z_4) \dots (z_i - z_p)}$ for $i=1, 2, \dots, p$

In local coordinates we considered linear element for which $p=2$ represented as follows



Finite element grid

Now ψ_i^e are the shape functions for this element (z_e, z_{e+1}) and are taken as:

$$\psi_1^e = \frac{z_{e+1} - z}{z_{e+1} - z_e} \text{ and } \psi_2^e = \frac{z - z_e}{z_{e+1} - z_e}, z_e \leq z \leq z_{e+1} \quad (39)$$

The finite element model of the equations for e^{th} element thus formed is given by

$$\begin{bmatrix} K^{11} \\ K^{21} \\ K^{31} \\ K^{41} \\ K^{51} \\ K^{61} \end{bmatrix} \begin{bmatrix} K^{12} \\ K^{22} \\ K^{32} \\ K^{42} \\ K^{52} \\ K^{62} \end{bmatrix} \begin{bmatrix} K^{13} \\ K^{23} \\ K^{33} \\ K^{43} \\ K^{53} \\ K^{63} \end{bmatrix} \begin{bmatrix} K^{14} \\ K^{24} \\ K^{34} \\ K^{44} \\ K^{54} \\ K^{64} \end{bmatrix} \begin{bmatrix} K^{15} \\ K^{25} \\ K^{35} \\ K^{45} \\ K^{55} \\ K^{65} \end{bmatrix} \begin{bmatrix} K^{16} \\ K^{26} \\ K^{36} \\ K^{46} \\ K^{56} \\ K^{66} \end{bmatrix} \begin{bmatrix} u^e \\ v^e \\ \omega_1^e \\ \omega_2^e \\ \theta^e \\ \varphi^e \end{bmatrix} + \begin{bmatrix} M^{11} \\ M^{21} \\ M^{31} \\ M^{41} \\ M^{51} \\ M^{61} \end{bmatrix} \begin{bmatrix} M^{12} \\ M^{22} \\ M^{32} \\ M^{42} \\ M^{52} \\ M^{62} \end{bmatrix} \begin{bmatrix} M^{13} \\ M^{23} \\ M^{33} \\ M^{43} \\ M^{53} \\ M^{63} \end{bmatrix} \begin{bmatrix} M^{14} \\ M^{24} \\ M^{34} \\ M^{44} \\ M^{54} \\ M^{64} \end{bmatrix} \begin{bmatrix} M^{15} \\ M^{25} \\ M^{35} \\ M^{45} \\ M^{55} \\ M^{65} \end{bmatrix} \begin{bmatrix} M^{16} \\ M^{26} \\ M^{36} \\ M^{46} \\ M^{56} \\ M^{66} \end{bmatrix} \begin{bmatrix} u^e \\ v^e \\ \omega_1^e \\ \omega_2^e \\ \theta^e \\ \varphi^e \end{bmatrix} = \begin{bmatrix} b^{1e} \\ b^{2e} \\ b^{3e} \\ b^{4e} \\ b^{5e} \\ b^{6e} \end{bmatrix} \quad (40)$$

Where $\{K^{mn}\}$ $[M^{mn}]$ and $\{u^e, v^e, \omega_1^e, \omega_2^e, \theta^e, \varphi^e, u^e, v^e, \omega_1^e, \omega_2^e, \theta^e, \varphi^e\}$ and $\{b^{me}\}$ $m, n=1,2,3,4,5,6$ denote the set of matrices of order 2×2 and 2×1 respectively and prime (') indicates $\frac{d}{dz}$. These matrices are defined as follows:

$$\left\{ \begin{array}{l} K_{ij}^{11} = -S \int_{z_e}^{z_{e+1}} \left(\psi_i^e \left(\frac{\partial \psi_j^e}{\partial z} \right) \right) dz - (1 + \Delta) \int_{z_e}^{z_{e+1}} \left[\left(\frac{\partial \psi_i^e}{\partial z} \right) \left(\frac{\partial \psi_j^e}{\partial z} \right) \right] dz + A_1 \int_{z_e}^{z_{e+1}} \left[\left(\psi_i^e \right) \left(\psi_j^e \right) \right] dz, \\ K_{ij}^{12} = -R \int_{z_e}^{z_{e+1}} \left(\psi_i^e \right) \left(\psi_j^e \right) dz, \quad K_{ij}^{13} = \Delta \int_{z_e}^{z_{e+1}} \left[\left(\psi_i^e \right) \left(\frac{\partial \psi_j^e}{\partial z} \right) \right] dz, \\ K_{ij}^{14} = -(Gr + Gm) \int_{z_e}^{z_{e+1}} \left(\psi_i^e \right) \left(\psi_j^e \right) dz, \quad K_{ij}^{15} = K_{ij}^{16} = 0 \\ M_{ij}^{11} = \int_{z_e}^{z_{e+1}} \left(\psi_i^e \right) \left(\psi_j^e \right) dz, \quad M_{ij}^{12} = M_{ij}^{13} = M_{ij}^{14} = M_{ij}^{15} = M_{ij}^{16} = 0, \end{array} \right. \quad (41)$$

$$\left\{ \begin{array}{l} K_{ij}^{21} = -S \int_{z_e}^{z_{e+1}} \left[\left(\psi_i^e \right) \left(\frac{\partial \psi_j^e}{\partial z} \right) \right] dz - (1 + \Delta) \int_{z_e}^{z_{e+1}} \left[\left(\frac{\partial \psi_i^e}{\partial z} \right) \left(\frac{\partial \psi_j^e}{\partial z} \right) \right] dz + A_1 \int_{z_e}^{z_{e+1}} \left[\left(\psi_i^e \right) \left(\psi_j^e \right) \right] dz, \\ K_{ij}^{22} = R \int_{z_e}^{z_{e+1}} \left(\psi_i^e \right) \left(\psi_j^e \right) dz, \quad K_{ij}^{23} = -\Delta \int_{z_e}^{z_{e+1}} \left[\left(\psi_i^e \right) \left(\frac{\partial \psi_j^e}{\partial z} \right) \right] dz, \quad K_{ij}^{24} = K_{ij}^{25} = K_{ij}^{26} = 0 \\ M_{ij}^{12} = 0, \quad M_{ij}^{22} = \int_{z_e}^{z_{e+1}} \left(\psi_i^e \right) \left(\psi_j^e \right) dz, \quad M_{ij}^{13} = M_{ij}^{14} = M_{ij}^{15} = M_{ij}^{16} = 0, \end{array} \right. \quad (42)$$

$$\left\{ \begin{array}{l} K_{ij}^{31} = -S \int_{z_e}^{z_{e+1}} \left[\left(\psi_i^e \right) \left(\frac{\partial \psi_j^e}{\partial z} \right) \right] dz, \quad K_{ij}^{32} = \lambda \int_{z_e}^{z_{e+1}} \left[\left(\frac{\partial \psi_i^e}{\partial z} \right) \left(\frac{\partial \psi_j^e}{\partial z} \right) \right] dz, \\ K_{ij}^{33} = 0, \quad K_{ij}^{34} = 0, \quad K_{ij}^{35} = 0, \quad K_{ij}^{36} = 0 \\ M_{ij}^{31} = 0, \quad M_{ij}^{32} = 0, \quad M_{ij}^{33} = \int_{z_e}^{z_{e+1}} \left(\psi_i^e \right) \left(\psi_j^e \right) dz, \quad M_{ij}^{34} = M_{ij}^{35} = M_{ij}^{36} = 0, \end{array} \right. \quad (43)$$

$$\left\{ \begin{array}{l} K_{ij}^{41} = -S \int_{z_e}^{z_{e+1}} \left[\psi_i^e \left(\frac{\partial \psi_j^e}{\partial z} \right) \right] dz, \quad K_{ij}^{42} = \lambda \int_{z_e}^{z_{e+1}} \left[\left(\frac{\partial \psi_i^e}{\partial z} \right) \left(\frac{\partial \psi_j^e}{\partial z} \right) \right] dz, \\ K_{ij}^{43} = 0, K_{ij}^{44} = 0, K_{ij}^{45} = 0, K_{ij}^{46} = 0 \\ M_{ij}^{41} = 0, \quad M_{ij}^{42} = 0, M_{ij}^{43} = 0, \quad M_{ij}^{44} = \int_{z_e}^{z_{e+1}} \left(\psi_i^e \right) \left(\psi_j^e \right) dz, \quad M_{ij}^{45} = M_{ij}^{46} = 0, \end{array} \right. \quad (44)$$

$$\left\{ \begin{array}{l} K_{ij}^{51} = -A_2 (1+\Delta) Ec \left[\int_{z_e}^{z_{e+1}} \left[\left(\psi_i^e \right) \left(\frac{\partial \bar{u}}{\partial z} \right) \left(\frac{\partial \psi_j^e}{\partial z} \right) \right] + \left(\frac{\partial \omega}{\partial z} \right)^2 \right] dz, \\ K_{ij}^{52} = (A_2 S - A_2 S Du Sc) \int_{z_e}^{z_{e+1}} \left[\left(\psi_i^e \right) \left(\frac{\partial \psi_j^e}{\partial z} \right) \right] dz, \quad K_{ij}^{53} = \int_{z_e}^{z_{e+1}} \left[\left(\frac{\partial \psi_i^e}{\partial z} \right) \left(\frac{\partial \psi_j^e}{\partial z} \right) \right] dz, \\ K_{ij}^{54} = K_{ij}^{55} = K_{ij}^{56} = 0, \\ M_{ij}^{51} = 0, \quad M_{ij}^{52} = 0, \quad M_{ij}^{53} = 0, \quad M_{ij}^{54} = 0, \quad M_{ij}^{55} = (A_2 Du Sc - A_2) \int_{z_e}^{z_{e+1}} \left(\psi_i^e \right) \left(\psi_j^e \right) dz, \quad M_{ij}^{56} = 0, \end{array} \right. \quad (45)$$

$$\left\{ \begin{array}{l} K_{ij}^{61} = -A_3 Pr Sc (1+\Delta) Ec \left[\int_{z_e}^{z_{e+1}} \left[\left(\psi_i^e \right) \left(\frac{\partial \bar{u}}{\partial z} \right) \left(\frac{\partial \psi_j^e}{\partial z} \right) \right] + \left(\frac{\partial \omega}{\partial z} \right)^2 \right] dz, \\ K_{ij}^{52} = (A_3 S Pr Sr - A_3 (1+F) S) \int_{z_e}^{z_{e+1}} \left[\left(\psi_i^e \right) \left(\frac{\partial \psi_j^e}{\partial z} \right) \right] dz, \quad K_{ij}^{53} = \int_{z_e}^{z_{e+1}} \left[\left(\frac{\partial \psi_i^e}{\partial z} \right) \left(\frac{\partial \psi_j^e}{\partial z} \right) \right] dz, \\ K_{ij}^{54} = K_{ij}^{55} = K_{ij}^{56} = 0, \\ M_{ij}^{51} = 0, \quad M_{ij}^{52} = 0, \quad M_{ij}^{53} = 0, \quad M_{ij}^{54} = 0, \quad M_{ij}^{55} = 0, \quad M_{ij}^{56} = (A_3 (1+F) - A_3 Pr Sr) \int_{z_e}^{z_{e+1}} \left(\psi_i^e \right) \left(\psi_j^e \right) dz, \end{array} \right. \quad (46)$$

$$\left\{ \begin{array}{l} b_i^{1e} = \left[\left(\psi_i^e \right) \left(\frac{\partial u}{\partial z} \right) \right]_{z_e}^{z_{e+1}}, \quad b_i^{2e} = \left[\left(\psi_i^e \right) \left(\frac{\partial v}{\partial z} \right) \right]_{z_e}^{z_{e+1}}, \quad b_i^{3e} = \left[\left(\psi_i^e \right) \left(\frac{\partial \omega_1}{\partial z} \right) \right]_{z_e}^{z_{e+1}} \\ b_i^{4e} = \left[\left(\psi_i^e \right) \left(\frac{\partial \omega_2}{\partial z} \right) \right]_{z_e}^{z_{e+1}}, \quad b_i^{5e} = \left[A_2 \left(\psi_i^e \right) \left(\frac{\partial \theta}{\partial z} \right) + Du \left(\psi_i^e \right) \left(\frac{\partial \varphi}{\partial z} \right) \right]_{z_e}^{z_{e+1}}, \\ b_i^{6e} = \left[A_3 \psi_i^e \left(\frac{\partial \varphi}{\partial z} \right) + Sr \psi_i^e \left(\frac{\partial \theta}{\partial z} \right) \right]_{z_e}^{z_{e+1}} \end{array} \right. \quad (47)$$

In general, to verify that the converged solutions are indeed correct, i.e. to guarantee grid (mesh) independency, a grid refinement test is carried out by dividing the whole domain into successively sized grids 81x81, 101x101 and 121x121 in the z -axis direction. Furthermore, the finite element code is run for different grid sizes and for a grid size of 101x101 the solutions are observed to achieve mesh independence. Therefore, for all subsequent computations, a grid size of

101 intervals is elected, with equal step size 0.01. At each node 6 functions are to be evaluated and after assembly of element equations, a set of 606 non-linear equations are obtained. These are solved with an iterative scheme by introducing the boundary conditions. Finally, the solution is assumed to be convergent whenever the relative difference between two successive iterations attains a prescribed value i.e. the iterative process is terminated when the following condition is fulfilled:

$$\sum_{i,j} |\xi^{n+1} - \xi^n| \leq 10^{-6} \quad (48)$$

where $\xi = u, v, \omega_1, \omega_2, \theta, \phi$ and n denotes the iterative step. This criterion maintains high accuracy for coupled multi-physical boundary layer equations. Once the key variables are computed, a number of wall gradient functions may be automatically evaluated.

4. General Numerical Validation with FEM

To verify accuracy of the generalized micropolar model with all parameters invoked. We employed the efficient finite element method (FEM) utilizing special symbolic packages such as MATLAB. FEM has found great popularity in modern engineering sciences and has been implemented in non-Newtonian flows. Table 1-3 presents the comparison between small perturbation method and FEM solutions for selected values of certain parameters. Excellent correlation is obtained. Confidence in the FEM solutions for the general micropolar transport model is therefore very high.

Tab 1. Comparison of $C_f, -C_w$ when $Ec = 0, Sr = 0$

				Olajuwon and Oahimire [15]		FEM results	
F	S	Du	R	C_f	$-C_w$	C_f	$-C_w$
0.5	2.5	0.02	0.5	-10.5322	3.6452	-10.533392	3.650223
1.0	2.5	0.02	0.5	-10.0297	3.7879	-10.029084	3.787772
0.5	5.0	0.02	0.5	-12.9772	6.5960	-12.976632	6.598060
0.5	2.5	1.0	0.5	-4.9692	3.7042	-4.967168	3.703866
0.5	2.5	0.02	1.0	-9.5204	7.2903	-9.518891	7.285592

Tab 2. Comparison of C_f , $-C_w$, Nu/Re_x and Sh/Re_x when $Ec = 0, Du = 0$

S	Kundu et al. [16]				FEM results			
	C_f	$-C_w$	Nu/Re_x	Sh/Re_x	C_f	$-C_w$	Nu/Re_x	Sh/Re_x
4.0	15.8370	2.73432	1.7040	0.4267	15.837004	2.734323	1.704011	0.426702
5.0	8.65130	1.52070	2.1300	0.5333	8.651306	1.520705	2.130014	0.533307
6.0	3.76030	0.92140	2.55697	0.6400	3.760304	0.921407	2.556974	0.640011

Tab 3. Comparison of C_f , $-C_w$, Nu/Re_x and Sh/Re_x when $B = 0, Ec = 0, Sr = 0, Du = 0$

R	K	M	S	Bakr and Chamkha [17]				FEM results			
				C_f	$-C_w$	Nu/Re_x	Sh/Re_x	C_f	$-C_w$	Nu/Re_x	Sh/Re_x
0.2	1.5	0.5	1.0	2.468	-0.18	1.0	0.22	2.466703	-0.175792	1.0	0.22
0.4	1.5	0.5	1.0	3.818	-0.615	1.0	0.22	3.809744	-0.614580	1.0	0.22
0.2	2.0	0.5	1.0	2.812	-0.144	1.0	0.22	2.810074	-0.143222	1.0	0.22
0.2	1.5	1.0	1.0	1.771	-0.148	1.0	0.22	1.765881	-0.146577	1.0	0.22
0.2	1.5	0.5	2.0	1.917	-0.401	1.0	0.44	1.916099	-0.393630	1.0	0.44

Tab 4. Effect of Δ, S, R, K, M on C_{fx}, C_{fy}, C_{wx} and C_{wy}

Δ	S	R	K	M	C_{fx}	C_{fy}	C_{wx}	C_{wy}
1.0	1.0	1.0	0.5	0.5	2.14534	0.43562	-0.038431	-1.23485
2.0	1.0	1.0	0.5	1.0	2.56235	0.74321	-0.022343	-1.32444
1.0	2.0	1.0	0.5	1.0	1.87355	0.42033	-0.04108	-1.54321
1.0	1.0	2.0	0.5	1.0	2.96542	0.36673	-0.056030	-1.06900
1.0	1.0	1.0	1.0	1.0	10.55431	4.42901	-0.08200	-1.69003
1.0	1.0	1.0	0.5	2.0	7.79678	2.35672	-0.046723	-1.64451

Tab 5. Effect of F, Ec, Du, Sr on Nu/Re_x and Sh/Re_x

F	Ec	Du	Sr	Nu/Re_x	Sh/Re_x
0.5	0.01	0.03	0.5	1.58731	0.35791
1.0	0.01	0.03	0.5	0.67322	0.34512
0.5	0.5	0.03	0.5	0.87033	0.44873
0.5	0.01	2.0	0.5	1.23972	0.81321
0.5	0.01	0.03	1.0	1.52095	0.19364

Inspection of Tables 4 reveals that a combination of negative and positive values, are observed for the primary and secondary components of skin friction and wall couple stress. There is therefore significant fluctuation in velocity and micro-rotation fields at the wall when secondary flow is present. This behavior is not captured in the absence of secondary effects. Table 5 reveals that as radiation parameter increases both Nusselt number and Sherwood number decrease in magnitude. Moreover, as Eckert, Dufour, Soret numbers increases, simultaneous decrease is observed in Nusselt number and increase in Sherwood number.

5. Graphical Results and Discussions

In order to gain a clear insight into the physical problem, numerical calculations for distribution of combined primary and secondary velocity, combined primary and secondary microrotation (angular) velocity, temperature and concentration for different values of the control parameters are illustrated in Figs. (2) - (17). In order to study the effects of pertinent parameters in fluid flow explicit computations were carried out by varying micro-rotation parameter Δ , dimensionless magnetic body force parameter M , permeability parameter K , rotation parameter R , suction parameter S , radiative-conduction parameter F , Eckert number Ec , Dufour number Du , and Soret number Sr . The following default parameter values are implemented in all the finite element computations $nt = \pi / 2, \varepsilon = 0.01, n = 10, Gr = 10, Gm = 4, M = 0.5, K = 5, Sc = 0.6, Pr = 0.7$. We do not explicitly consider oscillatory velocity influence since this has been thoroughly appraised in other studied – see Ganapathy [56].

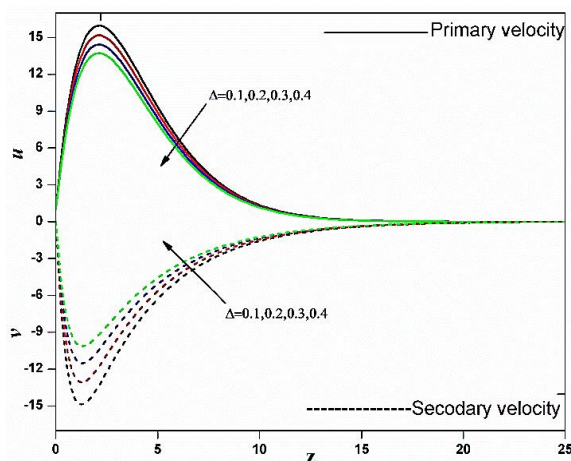


Fig.2. Velocity profiles for microrotation parameter.

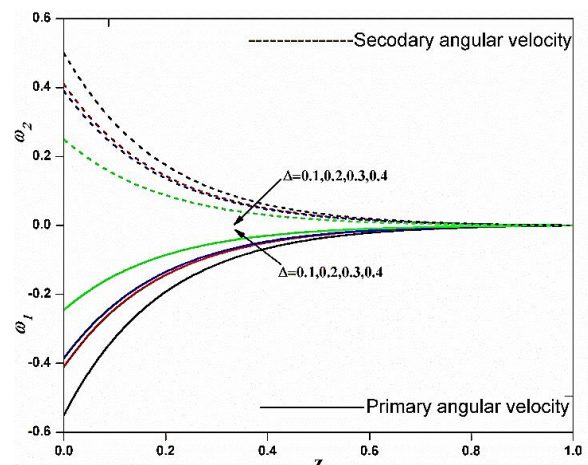


Fig.3. Angular velocity profiles for microrotation parameter.

Variations of viscosity ratio parameter Δ on u, v presented in the Fig. 2. With increasing vortex viscosity of micro-elements, u distribution is significantly reduced with transverse

coordinate (normal to the plate) with minimum acceleration computed a short distance from the plate surface. Conversely v is strongly accelerated and back flow is consistently observed indicating flow reversal. In addition, the angular velocity (Microrotation) distribution profiles are presented in the Fig. 3 presents consistent variations with an increment of Δ i.e., ω_1 increases and ω_2 decreases, which occurs due to the presence of increasing concentration of micro-elements which enhances vortex viscosity therefore also damps the gyratory motions of micro-elements. The maximum influence is at the wall since with greater concentration of micro-elements, these micro-elements are physically impaired from rotating near the boundary more than anywhere else in the fluid regime. This effect is progressively reduced with distance from the plate.

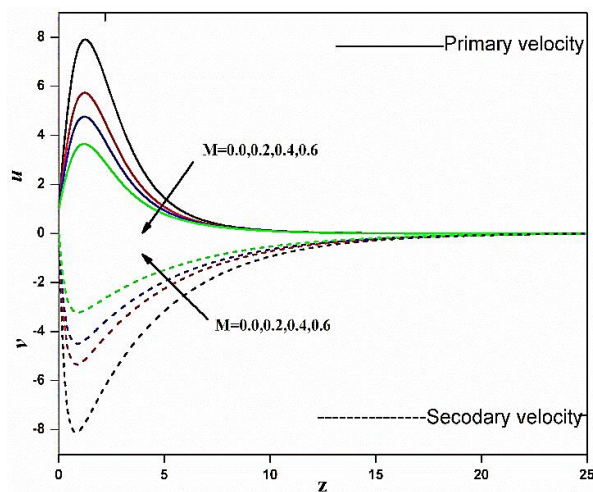


Fig.4. Velocity profiles for magnetic parameter.

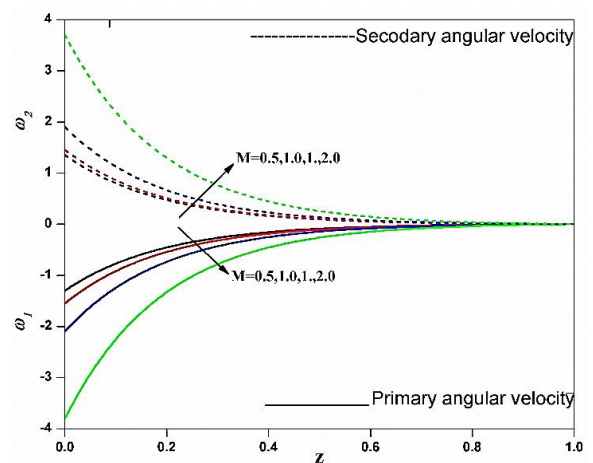


Fig.5. Angular velocity profiles for magnetic parameter.

Fig. 4 indicate that with increasing magnetic parameter M , there is a decrease in u and increasing v . The Lorentz magnetic drag force i.e. $-Mu$ in eqn. (11) is generated by the application of magnetic field in the z -direction (transverse to the primary velocity direction). This retards the primary flow whereas it accelerates the secondary flow via re-distribution in linear momentum. Significant flow alteration is therefore achieved with even a relatively weak increase in magnetic field. Maximum primary velocity and minimum secondary flow velocity therefore respectively correspond to $M = 0$ (vanishing magnetic field i.e. electrically non-conducting micropolar flow case). Fig. 5 present the influence of magnetic body force parameter M on ω_1 and ω_2 . The Lorentz drag component $-Mv$ in the secondary linear momentum eqn. (12) as expected induces a marked retardation in primary angular velocity via the coupling term, $+\Delta(\partial\omega_1/\partial z)$ which indirectly influences ω_1 . ω_2 increases with the increase of M since the term $-\Delta(\partial\omega_2/\partial z)$ couples the

secondary angular momentum field to the primary linear momentum field and the drag component, $-Mu$.

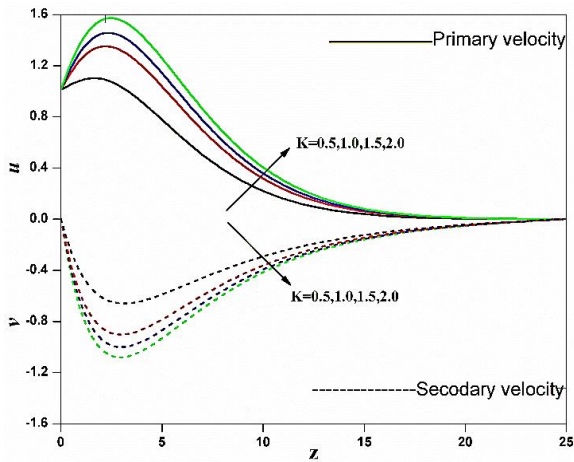


Fig.6. Velocity profiles for permeability parameter.

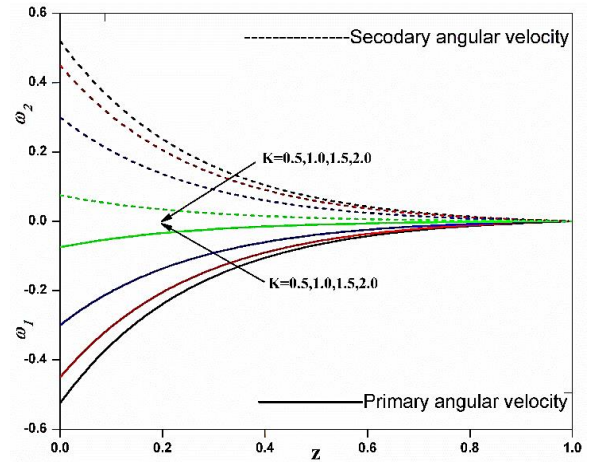


Fig.7. Angular velocity profiles for permeability parameter.

Fig. 6 present the impact of the porous medium permeability parameter (K) on both u, v . This parameter characterizes the hydraulic transmissivity of the porous medium. It arises in the Darcian drag force term in the primary and secondary linear momentum equations (11) and (12), via the terms, $-(1/K)u$ and $-(1/K)v$. With increasing permeability, the regime solid fibers progressively decrease. The Darcian bulk impedance to flow is therefore also decreased. This results in acceleration in the u and deceleration in v . The presence of a low permeability porous medium therefore damps the primary flow and boosts the secondary flow and vice versa for larger permeability media. Fig. 7 depicts the response in the angular velocity (micro-rotation) components to variation in permeability parameter (K). ω_1 is enhanced with greater permeability parameter i.e. the spin of micro-elements is damped with increasing porous material fibers. Conversely the ω_2 is accentuated indicating that micro-element spin (gyratory motion) is decreased with greater permeability.

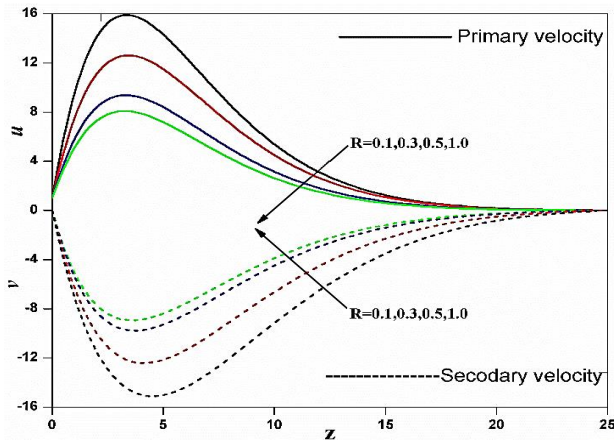


Fig.8. Velocity profiles for Rotation parameter.

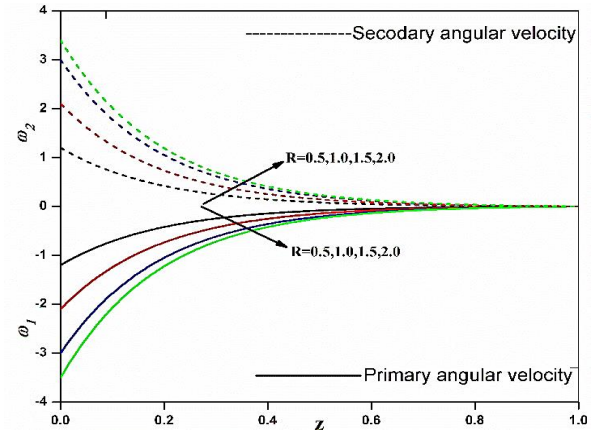


Fig.9. Angular velocity profiles for Rotation parameter.

Figs. 8-9 present the variations in u, v and ω_1, ω_2 with rotation parameter, R . The results show that rotation parameter R has minor decreasing effect on the u and conversely enhances the v . A reverse phenomenon is observed in ω_1, ω_2 i.e. ω_1 increases and ω_2 decreases as R increases. The rotational parameter, R , features in the so-called “cross flow terms”, $-Rv$ in the primary momentum eqn. (11) and $-Ru$ in the secondary momentum eqn. (12). As R increases the centrifugal force increases (faster angular velocity of rotation of the plate, Ω). The centrifugal effect influences each velocity field via the rotational body force term in the other velocity field equation. Although both terms are negative, only primary linear flow is decelerated and the compensation in momentum assists the secondary flow field. The micropolar coupling terms in both linear momenta equations i.e. $(1+\Delta)\partial^2 u / \partial z^2$, $(1+\Delta)\partial^2 v / \partial z^2$ and additionally the angular momentum coupling terms, viz. $-\Delta(\partial\omega_2 / \partial z)$ and, $+\Delta(\partial\omega_1 / \partial z)$ enable the rotational body force effect to impart a considerable influence on the micro-rotation field components. The primary spin of micro-elements is retarded whereas the secondary spin is effectively accelerated. Gyration is therefore substantially modified by rotational (centrifugal) body force.

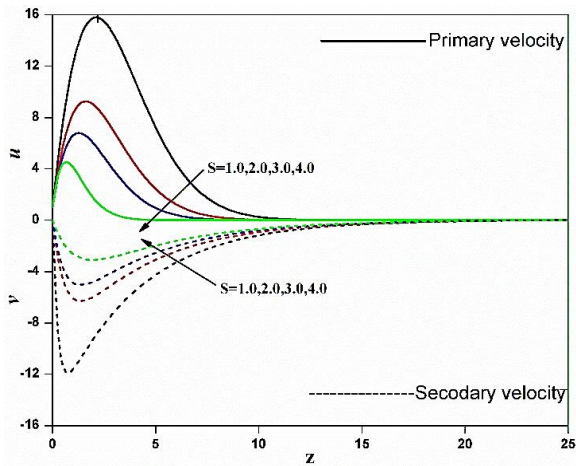


Fig.10. Velocity profiles for Suction parameter.

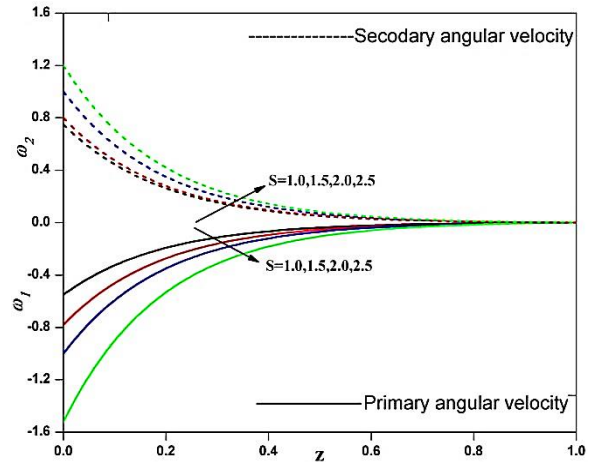


Fig.11. Angular velocity profiles for Suction parameter.

Figs. 10-11 present the response in u, v and ω_1, ω_2 profiles for various values of suction parameter S against spanwise coordinate, z . It is noticed that increasing suction significantly decreases u i.e. decelerates the boundary layer flow. Greater suction corresponds physically to removal of micropolar fluid via the wall. This destroys momentum, and causes the boundary layer to adhere to the wall thereby stabilizing boundary layer growth due to which the primary velocity of the fluid decreases, i.e., the flow is decelerated. But, the opposite behavior is produced by v . However, opposite behaviour is observed in case of injection. We note that the case $S < 0$ corresponds to blowing (mass injection) at the wall and is not relevant to the current study and has therefore not been addressed. A similar behaviour is observed in case of ω_1, ω_2 i.e. ω_1 decreases because angular momentum field (micro-rotation) retards gyratory motion (spin) of micro-elements which leads to a decrease and ω_2 accelerates gyratory motion (spin) of micro-elements which leads to increase.

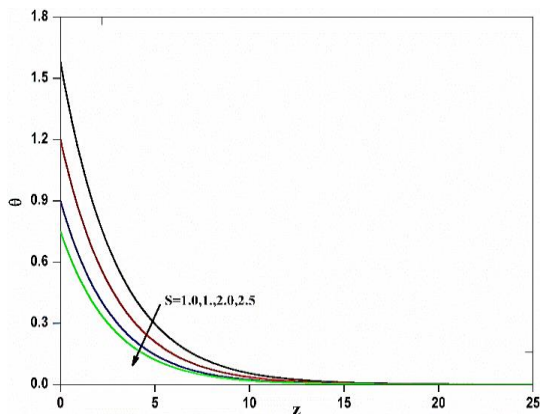


Fig.12. Temperature profiles for Suction parameter.

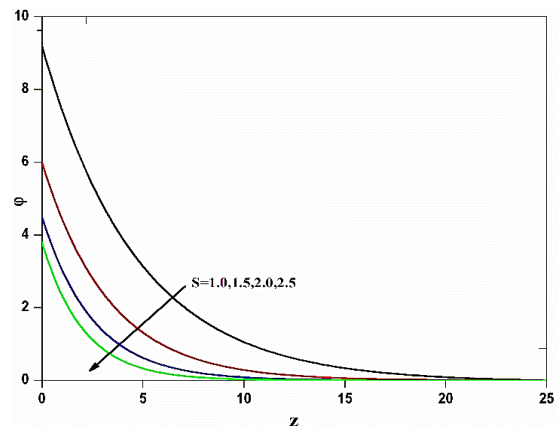


Fig.13. Concentration profiles for Suction parameter.

Figs. 12-13 depict the evolution in temperature (θ) and concentrations (ϕ) profiles with various suction parameter (s) values. Stronger wall suction significantly diminishes both temperature and concentration distribution, although a greater spread in profiles is computed over the same variation in suction parameter for concentration. Thermal boundary layer thickness and concentration (reactive solute) boundary layer thickness is therefore both reduced with enhanced wall suction. Again, asymptotically smooth convergence of profiles is achieved in the free stream confirming the imposition of a sufficiently large infinity boundary condition in the finite element program.

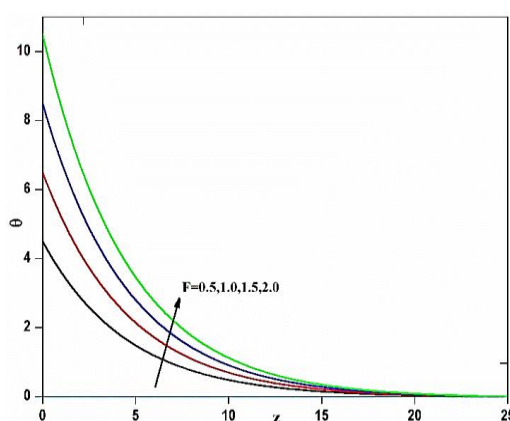


Fig.14. Temperature profiles for Thermal radiation parameter.

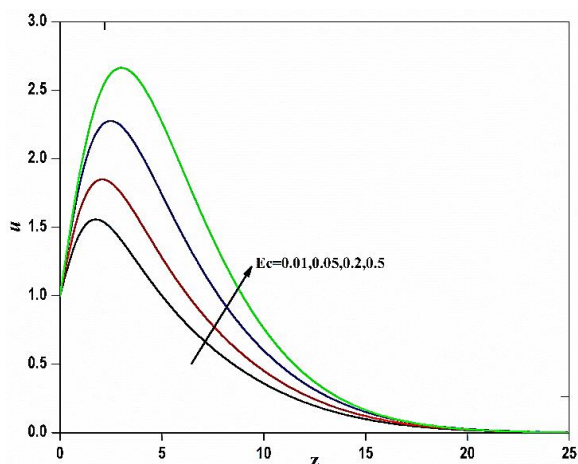


Fig.15. Velocity profiles for Eckert number

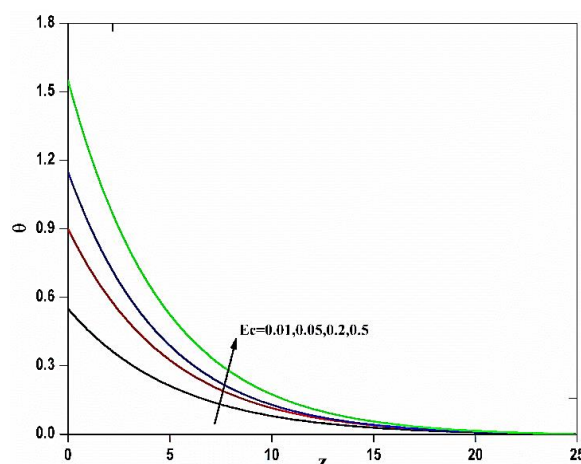


Fig.16. Temperature profiles for Eckert number.

Fig. 14 illustrates the influence of radiation-conduction parameter F on the temperature (θ). Increasing F values correspond to a greater contribution of thermal radiation heat transfer relative to thermal conduction heat transfer $F = 16 \bar{\sigma} T_{\infty}^3 / 3\kappa \bar{k}$. Fig. 13 indicates that with an increase of F the temperature profiles increases and this also increases thermal boundary layer thickness. The

F parameter arises solely in the dimensionless energy conservation equation, in the augmented thermal diffusion term, $\frac{1}{Pr}(1+F)\frac{\partial^2\theta}{\partial z^2}$. This serves to energize the flow with $F > 1$ for which thermal radiation contribution exceeds thermal conduction contribution. The supplementary heat flux assists in thermal transfer between fluid molecules. The case $F = 0$ physically represents vanishing thermal radiation and purely thermal conduction heat transfer and is therefore associated with minimal temperatures in the system.

Figs. 15-16 illustrate the influence of the Eckert number i.e. viscous dissipation parameter (Ec) on velocity and dimensionless temperature profiles. Ec expresses the relationship between the kinetic energy in the flow and the boundary layer enthalpy difference. It embodies the conversion of kinetic energy into internal energy by work done against the viscous fluid stresses. It is an important parameter for describing real working fluids in MHD energy generators and materials processing where dissipation effects are not trivial. Positive Eckert number corresponds to cooling of the wall (plate) and therefore a transfer of heat from the plate to the micropolar fluid. Convection is enhanced and we observe in consistency with that the fluid is accelerated i.e. linear (translational) velocity is increased in the micropolar fluid. Temperatures are also enhanced markedly with greater Eckert number, as shown in Figure 15 since internal energy is increased due to kinetic energy dissipation.

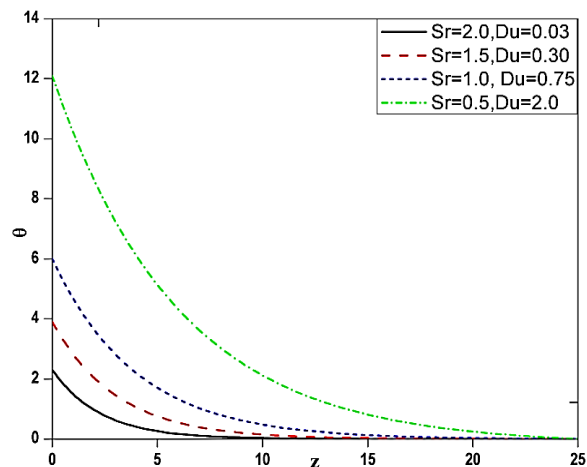


Fig.17. Temperature profiles for Soret and Dufour numbers.

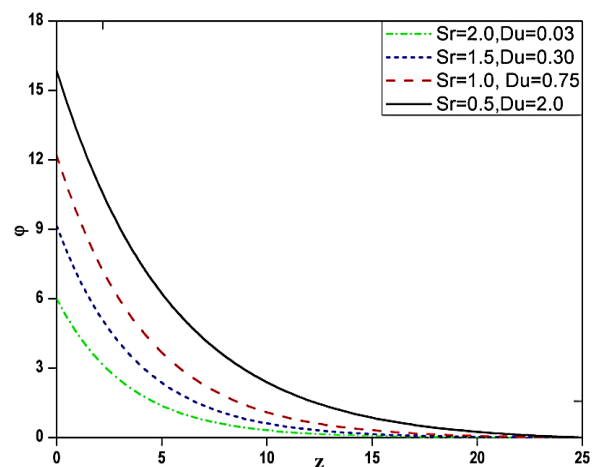


Fig.18. Concentration profiles for Soret and Dufour numbers.

Figs. 17-18 illustrate non-dimensional temperature and concentration profiles for different values of Sr and Du . It is clearly observed from the graph that the temperature distribution decreases whereas concentration profiles increase throughout the boundary layer with elevation in Sr and a decrease in Du . This is caused as a result of the mass flux created by the temperature

gradient and loss of temperature of the fluid. The concentration of the fluid increases due to the enhanced thermal diffusion rate. Furthermore, a diffusing species with higher values of Soret number (Sr) has a tendency to increase concentration profiles whereas thermal species with lower Dufour number (Du) values has the tendency of depreciating temperature profiles in the flow field. Hence temperature and concentration distributions are more influenced with the values of Sr and Du .

6. Concluding Remarks

An unsteady-state mathematical model has been presented for incompressible, free convection flow from a rotating vertical porous plate in a dissipative micropolar fluid with cross diffusion effects. Via non-dimensional quantities a boundary value problem has been derived in partial differential equation form, which are solved using Galerkin finite element method with weighted residual approach. Verification of solutions has been conducted against published literature. Selected computations have been visualized graphically and invoked parameter results are tabulated. The study has shown that:

- Translational (linear) (primary) flow is accelerated with increasing permeability parameter whereas it is damped (decelerated) with increasing microrotation (coupling) parameter, magnetic field parameter, wall suction parameter and rotation (centrifugal) parameter. But reverse phenomenon is observed in case of secondary flow.
- Angular velocity (gyration component) (primary) increases with microrotation (coupling) parameter and permeability parameter whereas the converse effect (deceleration) is induced with increasing magnetic body force parameter, rotation parameter and wall suction. But reverse phenomenon is observed in case of secondary flow.
- The temperature of the micropolar fluid and thermal boundary layer thickness are both increased with increasing conduction-radiation parameter and dissipation parameter (Eckert number) whereas the converse effect is induced
- Temperature distribution decreases whereas concentration profiles increase throughout the boundary layer with elevation in Soret and a decrease in Dufour number.

References

1. R. Tsai, J.S. Huang, Numerical study of Soret and Dufour effects on heat and mass transfer from natural convection flow over a vertical porous medium with variable wall heat fluxes, 2009, *Computational Materials Sciences*, vol. 47, pp. 23-30.

2. C.P. Chien, B.L. Mattes, Thermal Soret diffusion in the liquid phase epitaxial growth of binary III-V compounds, 1983, *J. Vac. Sci. Technol. B 1*, 648.
3. E. Blums, A. Mezulis, Thermal diffusion and particle separation in ferrocolloids, Transfer phenomenon in a magnetohydrodynamic and Electroconducting flows, 2010, *Fluid Mechanics and its Applications*, vol. 51, pp. 1-14.
4. D. Yadav, D. Nam, J. Lee, The onset of transient Soret-driven MHD convection confined within Hele-Shaw cell with nanoparticles suspension, 2016, *J. Taiwan Institute of Chemical Engineers*, vol. 58, pp. 235–244.
5. R.B. Dakhliya, V. Giovangigli, D.E. Rosner, Soret effects in laminar counter flow spray diffusion flames, 2002, *Combust theory modelling*, vol. 6, pp. 1-10.
6. F. Yang, C.K. Law, C.J. Sung, H. Zhang, A mechanistic study of soret diffusion in hydrogen-air flames, 2009, *47th AIAA Aerospace Sciences Meeting, New Horizons Forum and Aerospace Exposition*, Orlando, Florida, USA.
7. A. Postelnicu, Influence of a magnetic field on heat and mass transfer by natural convection from vertical surface in porous media considering Soret and Dufour effects, 2004, *Int. J. Heat Mass Transfer*, vol. 47, pp. 1467-1472.
8. M.S. Alam, M.M. Rahman, Dufour and Soret effects on MHD free convective heat and mass transfer flow past a vertical flat plate embedded in porous medium, 2005, *J. Naval Architecture and Marine Engineering*, vol. 21, pp. 55-65.
9. B. Vasu, N.B. Reddy, V.R. Prasad, O.A. Bég, Thermo-diffusion and Diffusion-Thermo effects on free convection flow past a semi-infinite vertical plate in the presence of suction and injection, 2013, *Int. J. Energy & Technology*, vol. 5, no. 14, pp. 1-11.
10. O.A. Bég, A.Y. Bakier, V.R. Prasad, Numerical study of free convection magnetohydrodynamic heat and mass transfer from a stretching surface to saturated porous medium with Soret and Dufour effects, 2009, *Computational Materials Science*, vol. 46, no. 1, pp. 57-65.
11. R.S. Tripathy, G.C. Dash, S.R. Mishra, M.M. Hoque, Numerical analysis of hydromagnetic micropolar fluid along a stretching sheet embedded in porous medium with non-uniform heat source and chemical reaction, 2016, *Eng. Sci. Tech: An Int. J*, Vol. 19, no. 3, pp. 1573-1581.
12. M.K. Partha, P.V.S.N. Murthy, G.P.R. Sekhar, Soret and Dufour effects in a non-Darcy porous medium, 2006, *ASME J. Heat Transfer*, vol. 128, pp. 605-610.
13. O.A. Bég, R. Bhargava, S. Rawat, E. Khaya, Numerical study of micropolar convective heat and mass transfer in a non-Darcy porous regime with Soret and Dufour effects, 2008, *Emirates J. Engineering Research*, vol. 13, pp. 51-66.

14. S.R. Mishra, S. Baag, D.K. Mohapatra, Chemical reaction and Soret effects on hydromagnetic micropolar fluid along a stretching sheet, 2016, *Eng. Sci. Tech.: An Int. J.*, Vol. 19(4), pp. 1919-1928.
15. B.I. Olajuwon, J.I. Oahimire, J.I, Unsteady free convection heat and mass transfer in an MHD micropolar fluid in the presence of thermo diffusion and thermal radiation, 2013, *Int. J. Pure and Applied Math*, vol. 84, no. 2,15-37.
16. P.K. Kundu, K. Das, S. Jana, MHD micropolar fluid flow with thermal radiation and thermal diffusion in rotating frame, 2015, *Bulletin Malaysia Mathematical Sciences Society*, vol. 38, pp. 1185-1205.
17. A.A. Bakr, A.J. Chamkha, Oscillatory free convection of a micropolar rotating fluid on a vertical plate with variable heat flux and thermal radiation, 2017, *Heat Transfer Reaserch*, vol. 48, no. 2, pp. 139-159.
18. S.M. Arifuzzaman, B.M.J. Rana, R. Ahmed, S.F. Ahmmed, Cross diffusion and MHD effect on a higher order chemically reactive micropolar fluid of naturally convective heat and mass transfer past through an infinite vertical porous medium with a constant heat sink, 2017, *AIP Conference Proceedings*, Vol. 1851, 020006.
19. J.N. Tokis, Free convection and mass transfer effects on the magnetohydrodynamic flows near a moving plate in a rotating medium, 1988, *Astro Phys. Space Sci*, vol. 44, no.12, pp. 291-301.
20. G. Nagaraju, M. Anjanna, K. Kaladhar, The effects of Soret and Dufour, chemical reaction, Hall and ion currents on magnetized micropolar flow through co-rotating cylinders, 2017, *AIP Advances*, Vol. 7, pp. 1-16.
21. A.A. Kendoush, Similarity solution for heat convection from a porous rotating disk in a flow field, 2013, *ASME J. Heat Transfer*, vol. 135, pp. 1885–1886.
22. P.V. Satya Narayana, B. Venkateswarlu, S. Venkataramana, Effect of Hall current and radiation absorption on MHD micropolar fluid in a rotating system, 2013, *Ain Shams Eng. J.*, vol. 4, pp. 843-854.
23. MD. Shamshuddin, O.A. Bég, S. Siva Reddy, A. Kadir, Rotating unsteady multi-physico-chemical magneto micropolar transport in porous media, 2017, *Computational Thermal Sciences.*, (In Press).
24. A.C. Eringen, *Micro-Continuum Field Theories: II-Fluent Media*, 2001, Springer, New York, USA.
25. S.K.L.L. Rao, N.Ch.P. Ramacharyulu, P. Bhujanga Rao, Slow steady rotation of a sphere in a micro-polar fluid, 1969, *Int. J. Eng. Sci*, vol. 7, pp. 905–916.

26. H. Ramkissoon, Slow steady rotation of an axially symmetric body in a micropolar fluid, 1977, *Appl. Sci. Res*, vol. 33, pp. 243–257.
27. A.D. Kirwan, M.S. Chang, On the micropolar Ekman problem, 1976, *Int. J. Engng. Sci*, vol. 14, pp. 685 -695.
28. V.U.K. Sastry, V.R. Mohan Rao, Micropolar fluid flow due to an oscillating plane subject to rotation, 1979, *Acta Mechanica*, vol. 33, pp. 45-53.
29. B. Mohanty, S.R. Mishra, H.B. Pattnaik, Numerical investigation on heat and mass transfer effect of micropolar fluid over a stretching sheet through porous media, 2015, *Alexandria Eng. J*, Vol. 54(2), pp. 223-232.
30. S.R. Mishra, G.C. Dash, P.K. Pattnaik, Flow of heat and mass transfer on MHD free convection in a micropolar fluid with heat source, 2015, *Alexandria Eng. J*, Vol. 54(3), pp. 681-689.
31. P.K. Rout, S.N. Sahoo, G.C. Dash, S.R. Mishra, Chemical reaction effect on MHD free convection flow in a micropolar fluid, 2016, *Alexandria Eng. J*, Vol. 55(3), pp. 2967-2973.
32. S. Baag, S.R. Mishra, G.C. Dash, M.R. Acharya, Numerical investigation on MHD micropolar fluid flow toward a stagnation point on a vertical surface with heat source and chemical reaction, 2017, *J. King Saud Eng. Sci.*, Vol. 29, pp. 75-83.
33. O.A. Bég, M.S. Khan, I. Karim, M.M. Alam, M. Ferdows, Explicit numerical study of unsteady hydromagnetic mixed convective nanofluid flow from an exponentially stretching sheet in porous media, 2014, *Appl. Nanoscience*, Vol. 4, pp. 943-957.
34. S.M. Arifuzzaman, M.S. Khan, K.E. Hossain, M.S. Alam, S. Akter, R. Roy, Chemically reactive viscoelastic fluid flow in presence of nano particle through porous stretching sheet, 2017, *Frontiers in Heat and Mass Transfer*, Vol. 9, no. 5, pp. 1-11.
35. M.S. Khan, M.M. Rahmana, S.M. Arifuzzaman, P. Biswas, I. Karim, Williamson fluid flow behaviour of MHD convective and radiative Cattaneo-Christov heat flux type over a linearly stretched surface with heat generation, viscous dissipation and thermal-diffusion, 2017, *Frontiers in Heat and Mass Transfer*, Vol. 9(15), 1-11.
36. R.S.R. Gorla, H.S. Takhar, Boundary layer flow of micropolar fluid on rotating axisymmetric surfaces with a concentrated heat source, 1994, *Acta Mechanica*, vol. 105, pp.1–10.
37. R.S.R. Gorla, Mixed convection of a micropolar fluid from a rotating cone, 1995, *Int. J. Heat and Fluid Flow*, vol. 16, pp. 69-73.
38. A. Nazir, S. Hussain, M. Shafique, The rotationally symmetric flow of micropolar fluids in the presence of an infinite rotating disk, 2015, *Appl. Math*. Vol. 6, pp. 430-439.
39. S. Deng, L. Hueng, J. Guan, M. Chen, Numerical investigation on the effects of pipe rotation on a dynamic hydro cyclone, 2017, *Chemical Engineering Transactions*, vol. 59, 1021-1-26.

40. N. Gajjela, S. Jangili, J.R.V. Murthy, O.A. Bég, Mathematical modelling of entropy generation in magnetized micropolar flow between co-rotating cylinders with internal heat generation, 2016, *Alexandria Engineering J.* vol. 55, pp. 1969-1982.
41. P. Biswas, S.M. Arifuzzaman, M.S. Khan, Effects of periodic magnetic field on 2D transient optically dense gray nanofluid over a vertical plate: A computational EFDM study with SCA, 2018, *Journal of Nanofluids*, Vol. 7, pp. 82-91.
42. S.M. Arifuzzaman, M.S. Khan, M.S. Islam, M.M. Islam, B.M.J. Rana, P. Biswas, S.F. Ahmmed, MHD Maxwell fluid flow in presence of nano-particle through a vertical porous-plate with heat-generation, radiation absorption and chemical reaction, 2017, *Frontiers in Heat and Mass Transfer*, Vol. 9(25), 1-11.
43. P.V. Kumar, S.M. Ibrahim, G. Lorenzini, Impact of thermal radiation and Joule heating on MHD mixed convection flow of a Jeffery fluid over a stretching sheet using homotopy analysis method, 2017, *Int. J. Heat and Technology*, vol. 35, no. 4, pp. 978-986.
44. J. Srinivas, S.O. Adesanya, J.A. Falade, G. Nagaraju, Entropy generation analysis for a radiative micropolar fluid flow through a vertical channel saturated with non-Darcian porous medium, 2017, *Int. J. Appl. Comput. Math.*
45. C.T. Lee, M.R. Mackley, P. Stonestreet, A.P.J. Middelburg, Protein refolding in an oscillatory flow reactor, 2001, *Biotechnology Letters*, vol. 23, pp. 1899-1901.
46. O.A Bég, S.K. Ghosh, M. Narahari, Mathematical modelling of oscillatory MHD Couette flow in a rotating highly permeable medium permeated by an oblique magnetic field, 2010, *Chem. Eng. Commun* vol. 198, pp. 235-254.
47. N. Reis, A.A. Vicente, J.A. Teixeira, M.R. Mackley, Residence times and mixing of a novel continuous oscillatory flow screening reactor, 2004, *Chem. Eng. Sci.* vol. 59, pp. 4967-4974.
48. R. Bhargava, R. Sharma, O.A. Bég, Oscillatory chemically-reacting free convection heat and mass transfer in a porous medium with Soret and Dufour effects: finite element modeling, 2009, *Int. J. Appl. Math. Mech.* Vol. 5, no. 6, pp. 15-37.
49. O.A Bég, S.K. Ghosh, S. Ahmed, T. A. Bég, Mathematical modelling of oscillatory magneto convection of a couple stress biofluid in an inclined rotating channel, 2012, *J. Mechanics in Medicine and Biology*, vol. 12, no. 3, pp. 1250050-1-1250050-35.
50. K. Maqbool, S. Ayesha, S. Idreesa, O.A. Bég, Analytical solutions for magnetohydro-dynamic oscillatory rotating plate and channel flows in porous media using a fractional Burgers viscoelastic model, 2016, *European Physical Journal Plus*, vol. 131, pp. 140-157.
51. T.K.V. Iynger, V.G. Vani, Oscillatory flow of a micropolar fluid generated by the rotary oscillations of two concentric spheres, 2004, *Int. J. Eng. Sci.* vol. 42, pp. 1035-1059.

52. B. Nayak, S. Baag, S.R. Mishra, Buoyancy effects on free convective MHD flow in the presence of Heat source/sink, *Modelling, Measurement and Control B*, vol. 86, pp. 14-32
53. Y. J. Kim, J.C. Lee, Analytical studies on MHD oscillatory flow of a micropolar fluid over a vertical porous plate, 2003, *Surface and Coating Technology*, vol. 171, pp. 187-193.
54. M. Modather, A.M. Rashad, A.J. Chamkha, An analytical study of MHD heat and mass transfer oscillatory flow of a micropolar fluid over a vertical permeable plate in porous medium, 2009, *Turkish. J. Eng. Env. Sci*, vol. 33, pp. 245-257.
55. M.D. Shamshuddin, T. Thirupathi, Soret and Dufour effects on unsteady MHD free convective flow of micropolar fluid with oscillatory plate velocity considering viscous dissipation effects, 2017, *Jurnal Teknlogi*, vol.79, no.4, pp. 123-136.
56. R. Ganapathy, A note on oscillatory Couette flow in a rotating system, 1994, *ASME J. Appl. Mech*, vol. 61, pp. 208-209.
57. J.N. Reddy, *An Introduction to the Finite Element Method*, 1985, McGraw-Hill, New York
58. K.J. Bathe, *Finite Element Procedures*, 1996, Prentice-Hall, New Jersey, USA.
59. Ö. Türk, M. Tezer-Sezgin, FEM solution to natural convection flow of a micropolar nanofluid in the presence of a magnetic field, 2017, *Meccanica*, vol. 52, pp. 889–901.
60. MD. Shamshuddin, O. Anwar Bég, M. Sunder Ram, A. Kadir, Finite element computation of multi-physical micropolar transport phenomena from an inclined moving plate in porous media, 2017, *Indian J. Physics*.

Nomenclature

- B_0 applied magnetic field strength
- C_f skin friction coefficient
- C_m wall couple stress
- C_p specific heat at constant pressure [$J Kg^{-1}K^{-1}$]
- C_s concentration susceptability [$mol m^{-3}$]
- C_w concentration of the solute at the plate [$mol m^{-3}$]
- C_∞ free stream concentration [$mol m^{-3}$]
- D_m molecular diffusivity [m^2s^{-1}]
- Du Dufour number
- Ec Eckert number
- F radiative-conduction parameter

g acceleration due to gravity [ms^{-1}]
 G_m solutal Grashof number
 G_r Grashof number
 J' micro inertia coefficient
 K permeability parameter
 K_t thermo-diffusion ratio [m^2s^{-1}]
 m_w concentration gradient
 n non-dimensional oscillation frequency
 Nu Nusselt number
 p constant pressure
 Pr Prandtl number
 q_r radiative heat flux [$W m^{-2}$]
 q_w constant heat flux
 R rotation parameter
 Re_x local Reynolds number
 S suction parameter
 Sc Schmidt number
 Sc Schmidt number
 Sh_x Sherwood number
 Sr Soret number
 t dimensionless time
 T temperature of the field in the boundary layer [K]
 T_m mean fluid temperature [K]
 T_w wall temperature of the fluid [K]
 T_∞ temperature of the fluid in free stream [K]
 u, v primary and secondary velocities
 ω_1, ω_2 primary and secondary angular velocities
 x' axis along the plate [m]
 y' axis perpendicular to the plate [m]

Greek symbols

- α Thermal diffusivity
- Δ microrotation parameter
- β_T volumetric coefficient of concentration expansion [K^{-1}]
- β_c volumetric coefficient of concentration expansion [K^{-1}]
- ρ density of micropolar fluid [$kg\ m^{-3}$]
- κ thermal conductivity [$Wm^{-1}K^{-1}$]
- $\bar{\kappa}$ mean absorption coefficient [m^{-1}]
- $\bar{\sigma}$ Stefan-Boltzmann constant [$Wm^{-2}K^{-4}$]
- ν Kinematic viscosity [m^2s^{-1}]
- μ fluid dynamic viscosity
- λ coefficient of gyro-viscosity [$kg\ m^{-1}s^{-1}$]
- γ gyroscopic viscosity
- ε small quantity
- θ dimensionless temperature
- ϕ dimensionless concentration
- ψ shape function
- ω microrotation component